Numerical simulation of the dynamics of freely falling discs

Article *in* Physics of Fluids · April 2013

DOI: 10.1063/1.4799179

3 authors, including:

MARCIN CHRUST
European Center For Medium Range Weather Forecasts
14 PUBLICATIONS **143** CITATIONS
SEE PROFILE

Jan Dusek
ICube Laboratory
78 PUBLICATIONS **1,249** CITATIONS
SEE PROFILE

Numerical simulation of the dynamics of freely falling discs

Marcin Chrust, Gilles Bouchet, and Jan Dušek

Citation: Phys. Fluids **25**, 044102 (2013); doi: 10.1063/1.4799179
View online: http://dx.doi.org/10.1063/1.4799179
View Table of Contents: http://pof.aip.org/resource/1/PHFLE6/v25/i4
Published by the AIP Publishing LLC.

PHYSICS OF FLUIDS **25**, 044102 (2013)

Numerical simulation of the dynamics of freely falling discs

Marcin Chrust,[1,a)] Gilles Bouchet,[2,b)] and Jan Dušek[1,c)]
[1]*Institut de Mécanique des Fluides et des Solides, Université de Strasbourg/CNRS, 2, rue Boussingault, 67000 Strasbourg, France*
[2]*Laboratoire IUSTI, Aix-Marseille Université/CNRS, 5, rue Enrico Fermi, 13453 Marseille Cedex 13, France*

(Received 5 November 2012; accepted 25 February 2013; published online 11 April 2013)

We present a comprehensive parametric study of the transition scenario of freely falling discs. The motion of the discs is investigated by a direct numerical simulation of the solid-fluid interaction. The discs are assumed to be homogeneous and infinitely thin. The problem is shown to depend on two independent parameters, the Galileo number expressing the ratio between effects of gravity and viscosity and the non-dimensionalized mass characterizing the inertia of the disc. The obtained results are in agreement with known experimental and numerical data and provide both detailed and comprehensive picture of the transition scenario in the two-parameter plane defined by the Galileo number and the non-dimensionalized mass. © *2013 American Institute of Physics*. [http://dx.doi.org/10.1063/1.4799179]

I. INTRODUCTION

Development of efficient numerical methods enabled recently[1] the understanding of the complete scenario of the transition of freely falling and ascending spherical particles. It was demonstrated that a sequence of well defined ordered states, depending on two dimensionless parameters, the Galileo number defined as

$$G_{sphere} = \tilde{G} = \frac{\sqrt{|\rho_s/\rho - 1|\, g d^3}}{\nu}, \tag{1}$$

and the solid to fluid density ratio ρ_s/ρ, and changing through bifurcations, leads to deterministic chaos. (In Eq. (1), ρ_s and ρ stand for the solid and fluid density, respectively, g is the gravitational acceleration, d the sphere diameter, and ν the kinematic viscosity.) The predicted scenario was confirmed to a large extent by experiments,[2] which evidenced qualitatively similar transitional regimes. In contrast with spherical particles, few numerical results exist for non-spherical bodies. In this paper, we focus our attention on freely falling infinitely thin discs (by a thin disc we understand a flat cylinder of infinite aspect ratio $\chi = h/d \to \infty$ where h is the thickness of the cylinder). Examples of motion of such bodies can be found in daily life. Everybody has observed the fluttering or tumbling motion of confetti falling in the air or of a coin dropped in water. Such behavior is intriguing in its own right, but is also important for the understanding of particle dispersion in many practical applications. Field *et al.*[3] interpreted the variety of motion regimes of falling discs, observed in their own and earlier[4,5] experiments, from the viewpoint of the theory of deterministic chaos.[6] They identified four distinct states depending on two dimensionless parameters, the non-dimensionalized moment of inertia $I^* = I/(\rho d^5)$ (I being the moment of inertia with respect to an axis lying in the plane of the disc) and the Reynolds number based on the mean vertical velocity. For low Reynolds numbers the fall was found to be steady and vertical. The wake remained axisymmetric. At higher Reynolds numbers, a periodic flutter was observed for small values of moment of inertia I^* and a

a)Electronic mail: marcin.chrust@uottawa.ca
b)Electronic mail: Gilles.Bouchet@univ-amu.fr
c)Electronic mail: dusek@unistra.fr

tumbling state was evidenced for higher values of I^*. The paths were found planar in both states. The fluttering state was characterized by the authors as periodic oscillations with the disc inclination angle ϕ, defined as the angle between its normal and the vertical direction, never exceeding $\pi/2$. The tumbling motion was described as a side-wise drifting of a disc rotating in a given direction. The authors could not determine if this state was truly periodic. The two mentioned states were found to be separated by a region of chaotic, intermittent states, characterized by a random switching between flutter and tumbling. The phase space spanned by I^* and Re was found to be covered by the four states in a non-overlapping manner. More recently,[7,8] small amplitude states preceding the onset of flutter, described as "possibly irregular or even chaotic" were evidenced experimentally. This experimental observation was confirmed later by direct numerical simulations (DNS) by Auguste,[9] who proved the existence of small amplitude non-vertical regimes preceding the appearance of large planar oscillations. The small amplitude regimes were recognized possibly responsible for the observed[8] delay of the onset of path oscillations of flat cylinders of high aspect ratio $\chi > 8$. A similar striking delay was already reported by Willmarth *et al.*[5] for discs with small inertia. Zhong *et al.*[10] observed non-planar trajectories. They identified two new types of motion, which they called spiral and transitional states, for discs having small moments of inertia I^*. They found that the initial planar zigzag motion was destabilized by the growth of a secondary oscillation in the normal direction. The direction of the rotation began to drift and the disc started to rotate about its symmetry axis which led eventually to a spiral motion. The axial rotation, essential for the appearance of the observed non-planar trajectories, can be triggered more easily for smaller I^* explaining why they were not reported for higher moments of inertia.

Numerical simulations have been recognized[7] to be better suited to distinguish an inherently chaotic behavior from experimental disturbances. In experiments, it is difficult to precisely control the physical properties of the system and the initial and boundary conditions. For instance, the fluid remains non-quiescent unless it is left to settle down for a sufficiently long time in between two observations. Long transients require large experimental set-ups allowing sufficiently long tracking of the fall of the bodies. Moreover, measurements of physical quantities in a non-intrusive manner are far from being trivial in most cases. This explains why direct numerical simulation has proved to be a very good tool for studying the transitional states of spherical particles.[1,11] However, the problem of both accurate and efficient, three-dimensional, simulation of falling discs and, more generally, flat bodies turned out to be a real numerical challenge.[7] The reason is the necessity to account for the essentially vertical far wake and the large oscillations or even continuous rotation of the body. A straightforward solution consists in considering a moving fully three-dimensional geometry.

In this paper, we employ an original domain decomposition technique to generalize the spectral–spectral-element method described in earlier papers.[1,12] The developed code is used to systematically explore the transition scenario of infinitely thin discs freely moving in a Newtonian fluid that is initially at rest.

II. MATHEMATICAL FORMULATION AND NUMERICAL METHOD

For an unconfined spherical body moving freely under the action of gravity, buoyancy, and hydrodynamic force in a Newton fluid initially at rest, an optimal numerical method consisting in accompanying its translational degrees of freedom by a vertically oriented cylindrical domain was used by Jenny *et al.*[1] This approach had the following advantages. It directly generalized the application of the spectral azimuthal decomposition shown[12] to mimic perfectly the onset of axisymmetry breaking in flows. Moreover, it allowed the wake to leave the computational domain through a remote cylinder basis on which an appropriate outflow condition minimized the influence of the boundary on the simulated physics. Finally, the spherical shape of the body allowed for a boundary fitted mesh enabling a considerable local refinement in the shear layers. The implicit coupling of the solid body and fluid equations made it possible to account for all solid to fluid density ratios (down to zero) degrading neither the accuracy of the time discretization nor the efficiency of the algorithm. In the case of a disc, a body-fitted mesh must follow the rotation of the body. However, this rotation affects the flow only at small distance from the body. In the fluttering regime, the wake

remains essentially vertical and is still best captured by a vertical domain. In the tumbling regime the wake is oblique but keeps a constant direction. In order to obtain a body fitted mesh close to the moving body and a cylindrical mesh translated along with the wake, the computational domain is decomposed into a relatively small spherical sub-domain rotating with the body, connected to the remaining cylindrical sub-domain by a spherical function expansion at the common interface. We adapted the fully implicit fluid-solid coupling described earlier[1] to the new configuration. The resulting numerical code remains both accurate and efficient in the same way as the version used for the simulation of a freely moving sphere. Here we present briefly the mathematical model and the numerical technique.

We assume the fluid to be incompressible and Newtonian with constant kinematic viscosity ν. The motion of a rigid homogeneous circular disc, of diameter d and of thickness that is negligible compared to its diameter, is assumed to be driven by gravity and buoyancy. This results in an effective gravitational acceleration $\mathbf{g}_{eff} = (1 - \rho/\rho_s)\mathbf{g}$, where $\mathbf{g}$ is the gravitational acceleration. The definition of $\mathbf{g}_{eff}$ covers both sedimenting and ascending discs. Note that the present definition differs by the factor ρ_s/ρ from that used for the simulation of freely moving spheres focusing mostly on the case of light spheres, i.e., $\rho_s/\rho < 1$. Ascending thin discs have small inertia and, from the viewpoint of parametric investigation, are equivalent to "infinitely light discs." The mathematical limit of cylinders of infinite aspect ratio $h \ll d$ requires, strictly speaking, $\rho_s/\rho \to \infty$. In experimental configurations this limit is often hard to achieve (e.g., in water) but, virtually in all cases of falling discs, the density ratio $\rho/\rho_s < 1$ has been used. The ratio $\rho/\rho_s < 1$ thus represents a more or less significant correction of the gravity. The fluid is assumed to adhere perfectly to the solid body surface. The fluid medium is considered infinite and quiescent far from the moving body.

The velocity vector is considered with respect to a fixed reference frame. The axes of the cylindrical sub-domain remain parallel to this fixed frame while those of the spherical sub-domain rotate. In this sub-domain the velocity field is described by its projection onto the local rotating frame. The outer boundary conditions are a Dirichlet (zero velocity) condition at the inflow boundary (bottom basis in Figure 1) and zero Neumann boundary conditions simulating no-stress conditions at the outflow (on top basis) and on the cylindrical surface.

The non-dimensionalization is based on the scale of the force resulting from the weight and buoyancy $(m - \rho V)\mathbf{g}$, where m is the mass and V the volume of the body. This force defines the velocity scale

$$v_{scale} = \sqrt{|m/\rho V - 1|gd}. \tag{2}$$

In that case, the fluid equations write

$$\frac{\partial \mathbf{v}}{\partial t} + [(\mathbf{v} - \mathbf{u} - \boldsymbol{\omega} \times \mathbf{r}) \cdot \nabla]\mathbf{v} + \boldsymbol{\omega} \times \mathbf{v} = -\nabla p + \frac{1}{G}\nabla^2 \mathbf{v} \tag{3}$$

and

$$\nabla . \mathbf{v} = 0, \tag{4}$$

where $\mathbf{u}$ is the translation velocity of the body center. $\boldsymbol{\omega}$ is the angular velocity of the rotating spherical sub-domain. The Galileo number G appearing in Eq. (3) is given by

$$G = \frac{\sqrt{|m^* - V^*|gd^3}}{\nu} = \frac{\sqrt{m^* g_{eff} d^3}}{\nu} \tag{5}$$

and m^* and V^* stand for the non-dimensionalized mass and volume of the body

$$m^* = \frac{m}{\rho d^3}, \quad V^* = \frac{V}{d^3}. \tag{6}$$

The solid body equations then write

$$m^* \left(\frac{d\mathbf{u}}{dt} + \omega \times \mathbf{u} \right) = \mathbf{F}_{fl}(\mathbf{v}, p) + \mathbf{k}_{fix}, \tag{7}$$

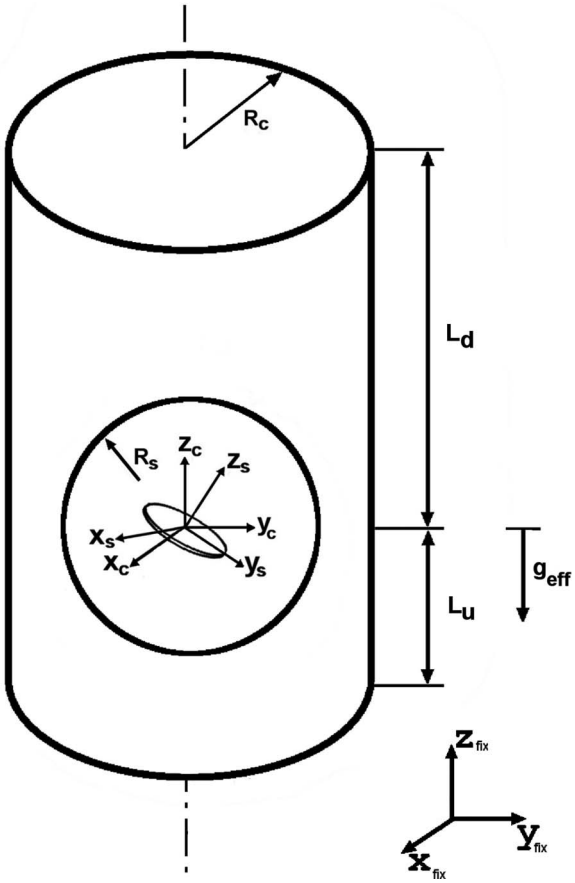

FIG. 1. Geometry of the problem. $\mathbf{g}_{eff}$—vertical vector of effective gravity oriented downward or upward for sedimenting or ascending bodies, (x_{fix}, y_{fix}, z_{fix}) fixed reference frame, (x_c, y_c, z_c) vertically translated frame, and (x_s, y_s, z_s) frame of the spherical sub-domain rotating with the body. Numerical parameters: radius of the spherical sub-domain: $R_s = d$, $R_c = 8d$, $L_u = 12d$, and $L_d = 25d$.

$$\alpha I^* \frac{d\Omega_z}{dt} = M_{fl_z}, \tag{8}$$

$$I^* \left(\frac{d\Omega_+}{dt} - i\alpha\Omega_+\Omega_z \right) = M_{fl_+}, \tag{9}$$

where $\mathbf{k}_{fix}$ is the vertical unit vector pointing upward or downward for sedimenting or ascending bodies, respectively. Equations (8) and (9) are written for complex ($U(1)^1$) coordinates of angular velocity $\Omega_+ = \Omega_x + \mathrm{i}\Omega_y$ and and torque $M_{fl+} = M_{flx} + \mathrm{i}M_{fly}$. The angular velocity vector of the spherical sub-domain has the components $\boldsymbol{\omega} = (\Omega_x, \Omega_y, 0)$. Due to the axisymmetry of the disc, the body fitted mesh is not required to follow the rotation about its axis. The complex coordinates uncouple Eqs. (8) and (9). The non-dimensionalized moment of inertia is defined in agreement with literature[3,5] as

$$I^* = \frac{I}{\rho d^5}. \tag{10}$$

In the case of an infinitely thin and homogeneous disc $\alpha = 2$ and $I^* = m^*/16$. The full system of Navier-Stokes equations (3) and (4) and of motion equations (7) through (9) depends on only two dimensionless parameters (G, m^*).

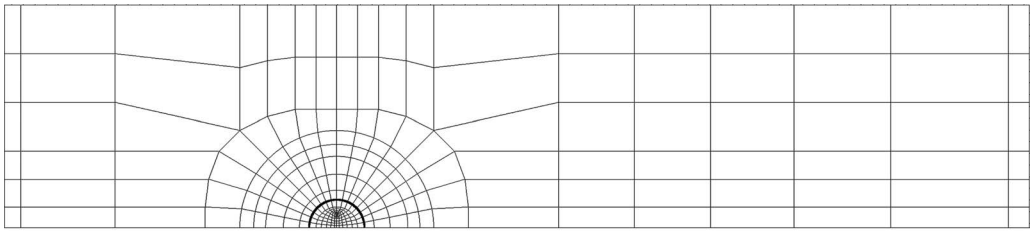

FIG. 2. Spectral element discretization of the radial-axial plane of the computational domain. The disc is represented by the segment of length 0.5 recognizable by the mesh refinement. The thick line marks the separation between the mesh of the spherical sub-domain and of the remaining mesh. The inflow is situated on the left. The cylindrical computational domain of radius $R = 8d$ extends $12d$ upstream and $25d$ downstream. The mesh contains $N_{el} = 278$ spectral elements containing 6×6 collocation points.

As mentioned above, the vertical cylindrical domain is decomposed into a spherical sub-domain and a remaining cylindrical part (see Figure 1). Both sub-domains are discretized by a Fourier azimuthal decomposition about their respective polar axes. The polar axis of the spherical sub-domain can rotate arbitrarily with respect to the polar axis of the cylinder. The axial-radial plane is discretized by a spectral element decomposition. The mesh is represented in Figure 2. A single mesh was generated to discretize both sub-domains. The separation is marked by the thick half-circle in Figure 2. The mesh is essentially the same as that used earlier for the investigation of instabilities of a fixed disc placed perpendicularly to the flow.[13] At that occasion, the sensitivity of the first two bifurcation thresholds to the variation of all numerical parameters, except those related to the domain decomposition, was extensively tested. It was shown that the choice of geometric parameters specified in the captions of Figures 1 and 2 ensures numerical convergence within a fraction of the Reynolds number of the computed instability thresholds. The effect of truncation of the azimuthal Fourier expansion was also tested and showed a very rapid convergence. In the present configuration, the same azimuthal Fourier truncation $m \leq M$ (where m denotes the azimuthal wave-number and M the largest value taken in account) is used in both sub-domains and both expansions are reconnected at the spherical interface by expansion into spherical functions $Y_{\ell,m}$ ($m \leq \ell$). The spherical function expansion is truncated at $\ell_{max} = M$. The details of the method are described in the recent Ph.D. thesis of Chrust.[14] This common truncation was thoroughly tested along with the value of the radius R_s of the spherical sub-domain appearing as a second parameter of the decomposition in several configurations.[14] For falling discs we chose to test the sensitivity of simulation of the flutter of a disc of non-dimensionalized mass $m^* = 0.1$. Table I shows that the instability threshold varies at most by a few tenth of the Galileo number value and the variation of the amplitude and frequency of developed oscillations at $G = 80$ is of the order of 0.1%. This means that the truncation at $\ell_{max} = 15$ is largely sufficient to ensure not only numerically converged results but also an independence of the choice of the radius of the spherical sub-domain (in the interval $1 \leq R_s \leq 3$). In what follows $\ell_{max} = 15$ and $R_s = 1$ are used. For further validation, numerical results of the Ph.D. thesis by Auguste[9] were used for comparison in Table II. The agreement is satisfactory in spite of two completely different numerical methods.

TABLE I. $A_{u_h}(G = 80)$ and $f_{u_h}(G = 80)$: amplitude and frequency of oscillations of horizontal velocity for a thin disc $\chi = \infty$, $m^* = 0.1$ at $G = 80$. G_{crit}: critical Galileo number.

R_s	ℓ_{max}	$A_{u_h}(G = 80)$	$f_{u_h}(G = 80)$	G_{crit}
1.00	15	0.9921	0.3801	64.11
1.00	31	0.9956	0.3796	64.19
2.00	15	0.9911	0.3799	64.41
2.00	31	0.9934	0.3794	64.17
3.00	15	0.9919	0.3798	...
3.00	15	0.9934	0.3795	...

TABLE II. Primary bifurcation thresholds expressed in terms of the Archimedes number $Ar = \sqrt{\frac{3}{4\pi}}G$ for a thin disc $\chi = \infty$. The third column contains results by Auguste.[9]

I^*	Ar_{cr}	Ar_{cr}[9]
0.004	36.15	33
0.012	25.71	24
0.048	16.69	16
0.160	14.64	14
0.480	17.26	14–18

The truncation $\ell_{max} = 15$ implies, as already stated, the truncation of the azimuthal expansion to $M = 15$. This is to be compared to $M = 7$, or less, sufficient for the simulation of axisymmetric geometries in comparable transitional regimes, such as those of the paper[13] presenting a very extensive parametric investigation of the transition scenario of fixed spheroids and cylinders. The computing costs are thus roughly multiplied by two which remains very reasonable compared to standard three-dimensional methods.

III. RESULTS

The transition scenario of freely falling discs can be characterized by a set of bifurcating asymptotic states. They correspond to stable asymptotic regimes reached in an infinite time horizon by the solid–fluid system for a fixed set of state parameters. In practical situations "infinite" means extremely diverse time scales given by the stability of the state. The latter decreasing dramatically close to bifurcations and at the onset of chaos, not all bifurcating states are really observable in laboratory experiments. Direct numerical simulation makes it possible to reach asymptotic states. Moreover, in DNS, all boundary conditions are under control and the perturbations are limited to a low and well controlled numerical noise due to rounding errors. As the result, DNS is able to unveil many new features and provide both a detailed and global view of the transition scenario. The present work was facilitated by the low computing costs of the used numerical algorithm and by the presence of only two governing dimensionless parameters: G, m^*. This section is organized as follows. In Sec. III A we present the morphology of the states identified in the investigated domain $25 \leq G \leq 500$ and $0 \leq m^* \leq 10$ of the parameter plane. In Sec. III B we describe the state diagram characterizing the transition scenario in the (m^*, G) plane. Finally we discuss the found transition scenario in Sec. III C.

A. States present in the scenario of the transition to chaos

The scenario is characterized by a limited number of bifurcating states for which we attempt to provide a quantitative description in terms of the following quantities wherever they apply: the amplitude of the path oscillations in the horizontal direction Δs, the mean horizontal and vertical velocities $\overline{u}_h$ and $\overline{u}_z$, and their amplitudes of oscillations Δu_h and Δu_v, respectively, the inclination angle ϕ, defined as the angle between the axis of the disc and the vertical direction and its maximum value ϕ_{max}, the angular velocity of rotation (about a horizontal axis) ω_h, the Strouhal number $St = fd/u_z$, where f is the oscillation frequency (obtained mostly from the horizontal velocity). The Reynolds number used by other authors[3,8] is obtained by multiplying the Galileo number by $\overline{u}_z$.

The simplest—steady vertical—state is characterized by $\overline{u_h} = \Delta u_h = \Delta u_v = \phi_{max} = \omega_h = \Delta s = St = 0$. The terminal velocity $u_\infty = u_z$, equivalent to a constant terminal Reynolds number, depends only on the Galileo number and can be obtained by a simple axisymmetric computation by determining the drag compensating the weight and buoyancy of the disc.

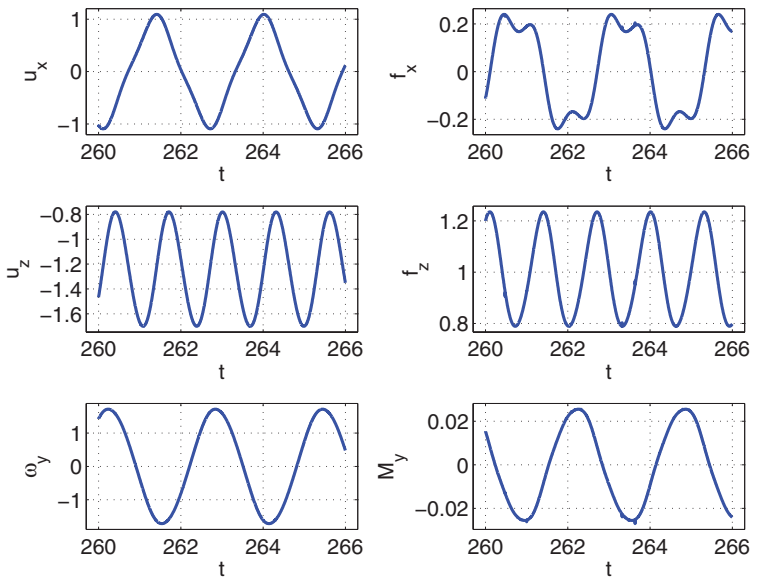

FIG. 3. $m^* = 0.1$, $G = 90$. (Top) Horizontal component of the velocity u_x and hydrodynamic force f_x; (middle) vertical component of the velocity u_z and of the force f_z; and (bottom) angular velocity ω_y and torque M_y. The y-axis is perpendicular to the trajectory plane.

1. Periodic fluttering state

The trajectory of the fluttering state lies in a plane arbitrarily selected by initial conditions. The average direction of the trajectory is vertical and the disc center describes a zig-zagging path about the vertical direction. Its symmetry axis rotates with an angular velocity normal to the plane of the trajectory and oscillates about zero with values not exceeding 90°. The period of oscillations of u_h, ω_h, and ϕ is the same, while the vertical velocity u_z oscillates with a double frequency. The onset of this state was tracked by observing one of the mentioned parameters, usually the horizontal velocity u_h. Figures 3 and 4 show a well established fluttering state by representing the velocities $u_h \equiv u_x$ (top-left), u_z (middle-left), and the angular velocity ω_y (bottom-left) for $m^* = 0.1$ at $G = 90$. Both Δu_h and Δu_z in the saturated state have a constant non-zero value. The period of oscillations of u_x and ω_y is 2.606 (in units d/v_{scale} where the velocity scale is defined by Eq. (2)). This corresponds to a non-dimensional frequency of 0.384 and, with account of the mean value -1.241 of the vertical velocity, to a Strouhal number equal to $St = 0.309$. The right column of

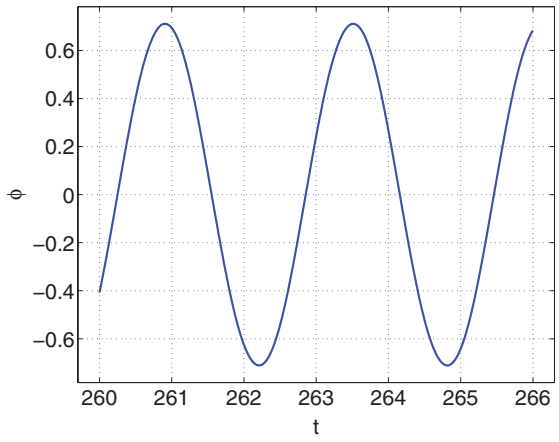

FIG. 4. $m^* = 0.1$, $G = 90$: inclination of the disc defined as an angle between the disc axis and the vertical direction.

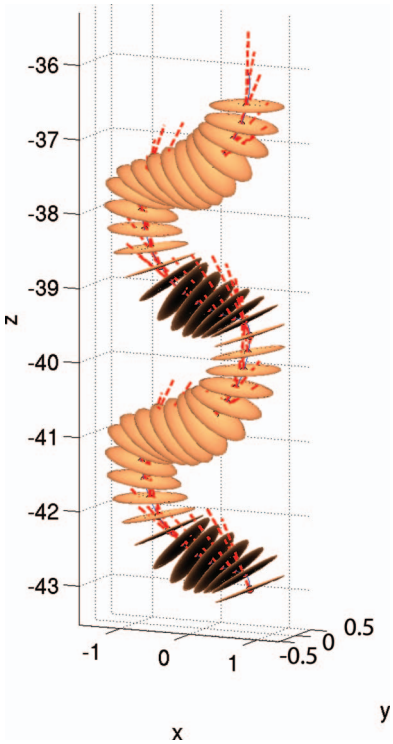

FIG. 5. Fluttering periodic state, $m^* = 0.1$, $G = 200$, z—vertical position, and x, y—horizontal positions as multiples of d. The dashed line represents a half-axis of the disc.

Figure 3 shows the hydrodynamic force and torque. The latter have the same period and reflect the same behavior. The system behaves like a low-dimensional dynamical system, the state of which can be characterized by any quantity. The inclination angle of the disc with respect to the vertical direction (Figure 4) is also a very practical characteristic.

Figure 5 shows a typical trajectory in the form of a sequence of snapshots in the way used in experimental image processing. The disc oscillates periodically back and forth. The maximum angle of inclination ϕ_{max} does not exceed $\pi/2$. Otherwise, the disc flips over the edge and starts to tumble. It is interesting to note that the amplitude of the vertical velocity oscillations can exceed the mean value. For example, for $m^* = 0.1$ and $G > 200$ we observed that, as the disc approached its extreme lateral position, it began to climb.

For small m^* ($m^* \leq 0.1$) the maximum inclination angle of the disc ϕ_{max} never exceeds $\pi/2$. For example, for $m^* = 0$ it reaches a maximum value of slightly less than 24° at $G = 200$ and decreases to 22° at $G = 500$ (see Figure 6(a)). In contrast, when the fluttering state gives way to tumbling (intermittent) the maximum angle grows to $\pi/2$ and the disc starts to tumble. This provides a useful method for delimiting precisely the stability of the fluttering state (see Figures 6(a) and 6(c)).

Figure 7 shows the wake of a disc in a saturated periodic fluttering regime for $m^* = 0.1$ at $G = 200$ by representing the axial vorticity iso-surfaces at levels 0.9. In one oscillation period a pair of vortices is shedded from the disc, each with the opposite orientation. The oscillating motion of the disc considerably enhances the mixing in the wake which is much shorter than for a sphere at a comparable mean Reynolds number. (The Reynolds number of the fall generating the wake in Figure 7 is 240—see Table III.)

The simulated regimes are reported in the state diagram 22 as symbols in the two parameter G, m^* plane. The information conveyed by the diagram is however incomplete because it is limited to the stability limits of different regimes. In order to provide a more accurate quantitative information potentially useful for other numerical simulations and experimental observations we sum up the obtained quantitative data in tables. Table III presents the data characterizing some selected periodic fluttering states.

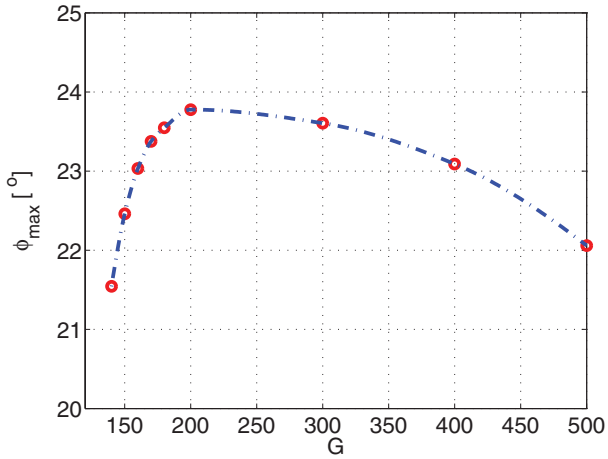

(a)

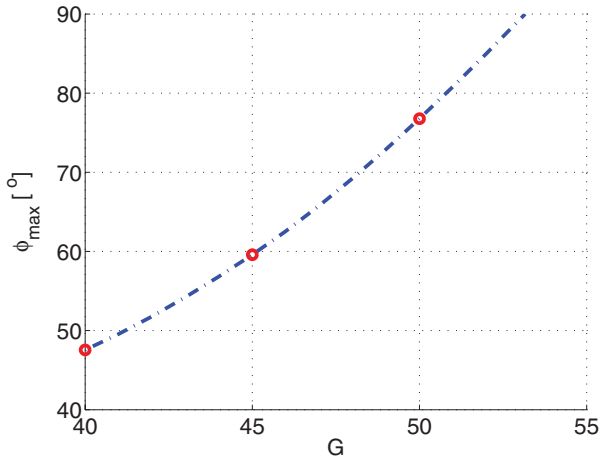

(b)

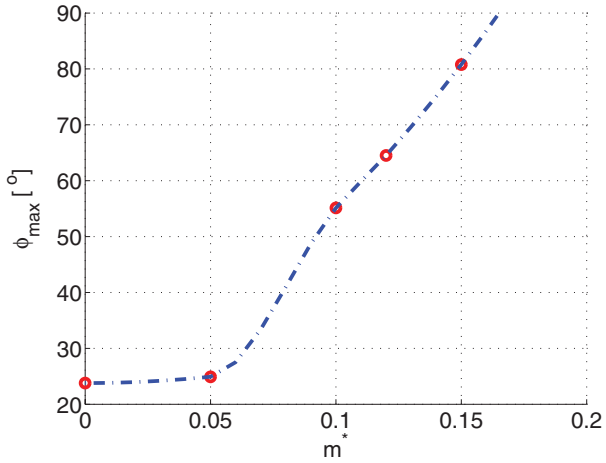

(c)

FIG. 6. (a) Fluttering periodic state, $m^* = 0$. Maximum inclination of the disc ϕ_{max} as a function of the Galileo number. (b) Same as in figure (a) for $m^* = 0.75$. The limit of stability of the fluttering state can be estimated at $G \approx 53.5$. (c) $G = 200$, maximum inclination angle as a function of m^*. The disc starts to tumble at $m^* \approx 0.163$.

TABLE III. Some quantitative data for selected periodic fluttering states. Meaning of symbols: $\overline{u}_z$—mean vertical velocity; Δu_z, Δu_h, $\Delta\omega_h$—amplitude of oscillations of the vertical and horizontal component of velocity and of the angular velocity, respectively; $\Delta s = \sqrt{(s_x^2 + s_y^2)}$—maximum horizontal displacement, where s_x and s_y are displacements in the x- and y-direction, respectively; St—the Strouhal number; and ϕ_{max} is the maximal inclination of the disc.

m^*	G	$\overline{u}_z$	Δu_z	Δu_h	$\Delta\omega_h$	$\Delta s/d$	St	ϕ_{max} (rad)
0	140	−1.376	0.271	1.024	1.381	0.271	0.426	0.380
0	150	−1.374	0.307	1.109	1.467	0.287	0.437	0.392
0	160	−1.362	0.333	1.177	1.526	0.298	0.446	0.401
0	170	−1.371	0.356	1.237	1.570	0.308	0.454	0.408
0	180	−1.367	0.377	1.296	1.608	0.317	0.464	0.414
0	200	−1.363	0.401	1.380	1.649	0.328	0.477	0.415
0	300	−1.343	0.476	1.682	1.712	0.370	0.528	0.407
0	400	−1.328	0.530	1.885	1.709	0.399	0.562	0.390
0	500	−1.292	0.546	2.035	1.693	0.411	0.598	0.380
0.05	75	−1.316	0.225	0.733	1.240	0.266	0.317	0.466
0.05	80	−1.307	0.292	0.854	1.420	0.299	0.326	0.523
0.05	90	−1.301	0.370	1.001	1.588	0.338	0.330	0.578
0.05	100	−1.285	0.423	1.108	1.6781	0.366	0.345	0.599
0.1	80	−1.250	0.408	0.991	1.648	0.370	0.304	0.685
0.1	90	−1.241	0.460	1.093	1.718	0.400	0.310	0.711
0.1	100	−1.232	0.502	1.181	1.759	0.427	0.306	0.731
0.1	200	−1.199	0.972	2.097	1.863	0.797	0.292	0.962
0.1	300	−1.255	1.333	2.778	1.876	1.199	0.246	1.102
0.1	400	−1.291	1.601	3.297	1.855	1.578	0.216	1.174
0.1	500	−1.339	1.839	3.759	1.826	1.974	0.190	1.227
0.25	90	−1.347	0.924	1.602	2.213	0.749	0.182	1.362
0.5	38	−1.166	0.106	0.343	0.865	0.209	0.208	0.555
0.5	50	−1.254	0.365	0.737	1.626	0.410	0.184	1.057
0.75	45	−1.271	0.284	0.595	1.482	0.379	0.154	1.040
0.75	50	−1.377	0.432	0.774	1.791	0.527	0.131	1.340
1	40	−1.222	0.160	0.396	1.107	0.287	0.160	0.867
2	34	−1.165	0.043	0.173	0.568	0.165	0.137	0.532
2	38	−1.243	0.095	0.267	0.856	0.251	0.123	0.822
10	45	−1.250	0.006	0.050	0.173	0.094	0.067	0.332

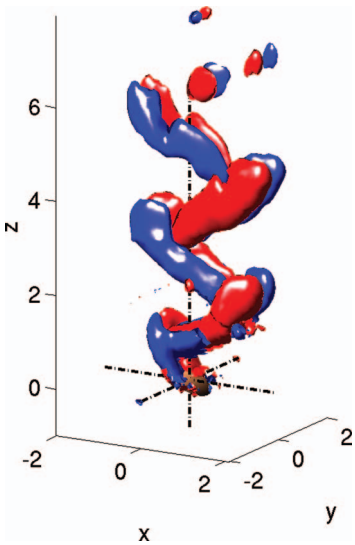

FIG. 7. Fluttering periodic state, $m^* = 0.1$, $G = 200$. Axial vorticity iso-surfaces at levels ± 0.9.

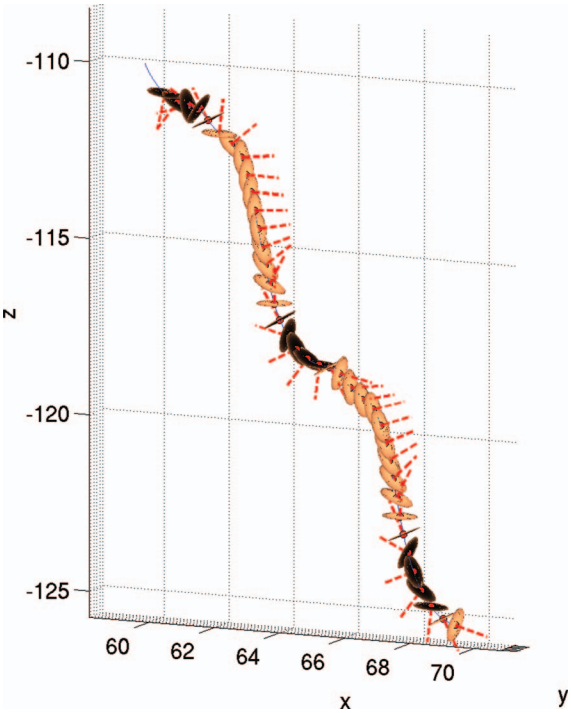

FIG. 8. Tumbling state, $m^* = 0.5$, $G = 160$, z—vertical position, x, y—horizontal positions as multiples of d. The dashed line represents a half-axis of the disc.

2. Tumbling state

The flutter does not usually transit directly to a stable tumbling state but switches intermittently from flutter to tumbling which results in an intermittent chaos described in Sec. III A 3. The exactly periodic tumbling state is characterized by the rotation of the disc over edge in one direction. This results in an oblique trajectory. The angular velocity ω_h and the horizontal velocity u_h are oscillating functions of time with a non-zero mean value characterizing the rotation direction and the horizontal drift. Two typical situations are encountered. Discs with moderate inertia, $m^* < 0.75$, go through distinct phases of rotation and flight over edge (see Figure 8). Figure 9 shows u_x (top-left), u_z (middle-left), and ω_y (bottom-left) and Figure 10 represents the, now monotonically varying, inclination angle ϕ for $m^* = 0.5$ at $G = 160$. The components of the hydrodynamic force and the torque are represented in the right column of Figures 9. Note that the y-axis is perpendicular to the trajectory plane. As can be seen from the figure, two (negative) peaks of vertical velocity u_z (a larger followed by a smaller one) correspond each to a half turn. During this phase, the disc practically does not fall and, during the first half turn, it reaches the maximal horizontal velocity. After completion of the turn, the angular velocity reaches a zero value. The horizontal velocity passes through a minimum before starting to increase gradually while the vertical velocity strongly accelerates. The rotation angle lies clearly midway between the dotted lines marking the vertical position of the disc axis, i.e., the disc axis is horizontal. For discs with substantial inertia the oscillations of the above mentioned quantities, that is u_h, u_z, and ω_h, are practically harmonic (see Figure 11) and amplitudes of oscillations of the velocities are small compared to their mean values. The disc describes a practically rectilinear oblique trajectory while rotating with almost constant angular velocity about a horizontal axis (Table IV).

Figure 12 shows the vortical structures in the wake of a disc in a tumbling regime for $m^* = 0.5$ at $G = 160$ by representing the axial vorticity iso-surfaces at levels ± 1.1. The rotation of the disc generates a very significant mixing in the wake. The wake is thus very short. For this reason it was unnecessary to align the axis of the cylindrical domain with the mean path direction.

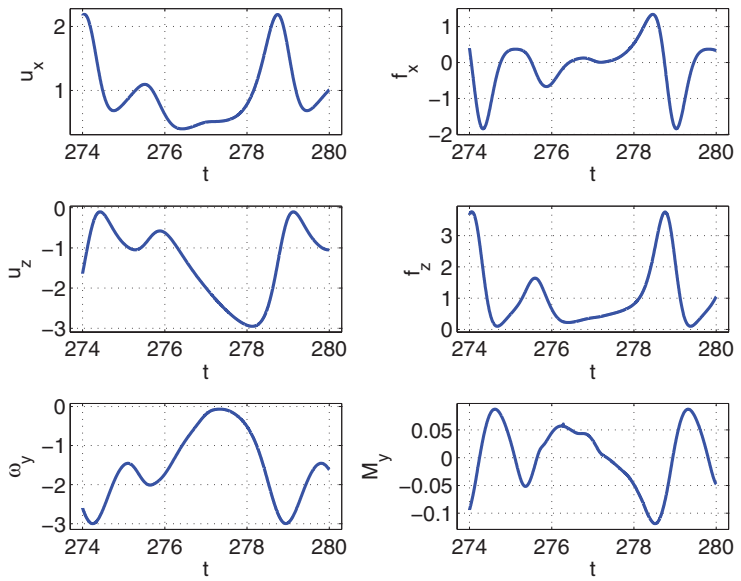

FIG. 9. $m^* = 0.5$, $G = 160$. (Top) Horizontal component u_x of the velocity and hydrodynamic force f_x; (middle) vertical component u_z of the velocity and of the force f_z; (bottom) angular velocity ω_y and torque M_y. The y-axis is perpendicular to the trajectory plane.

3. Intermittent and tumbling—Zig-zagging regimes

For $m^* < 2$, the tumbling and periodic fluttering states are separated by a region of intermittent states. In this region none of both states is stable. The flutter is no longer limited to amplitudes of inclination smaller than 90° and the tumbling is not yet stable enough to persist in a periodic regime. The rotation stops at irregular intervals and changes the direction. The duration of tumbling stages is clearly random in Figure 13 showing the horizontal velocity u_h (top) and angular velocity ω_h

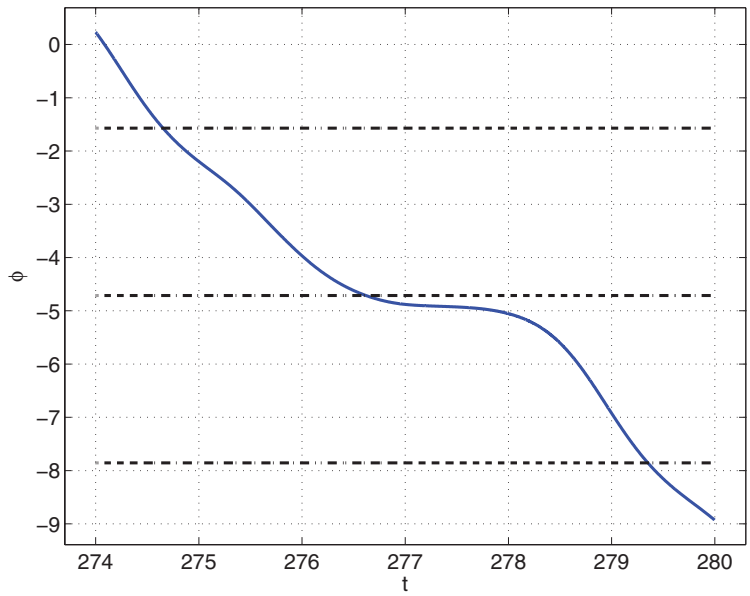

FIG. 10. $m^* = 0.5$, $G = 160$: inclination of the disc defined as an angle between the disc axis and the vertical direction. The dashed-dotted horizontal lines mark the position when the disc axis is horizontal.

TABLE IV. Some quantitative data for selected tumbling states from the state diagram of Figure 22. Meaning of symbols: $\overline{u}_z$, $\overline{u}_h$, and $\overline{\omega}_h$—mean vertical, horizontal, and angular velocity; Δu_z, Δu_h, $\Delta\omega_h$—amplitude of oscillations of the vertical and horizontal component of velocity and of the angular velocity, respectively; St—the Strouhal number; and α—mean angle with respect to vertical direction.

m^*	G	$\overline{u}_z$	Δu_z	$\overline{u}_h$	Δu_h	$\overline{\omega}_h$	$\Delta\omega_h$	St	α
0.75	90	−1.224	0.504	−0.929	0.351	1.292	0.721	0.315	33.96
0.75	100	−1.202	0.534	−0.929	0.349	1.317	0.689	0.333	34.83
0.75	120	−1.159	0.485	−0.940	0.349	1.393	0.632	0.366	36.48
0.75	140	−1.126	0.472	−0.941	0.347	1.442	0.592	0.392	37.49
0.75	160	−1.101	0.466	−0.943	0.346	1.480	0.567	0.412	38.08
0.75	200	−1.067	0.461	−0.941	0.347	1.533	0.538	0.443	38.74
0.75	300	−1.014	0.451	−0.939	0.343	1.599	0.502	0.490	40.73
0.75	400	−0.987	0.449	−0.937	0.344	1.626	0.487	0.515	41.56
1	80	−1.267	0.424	−0.631	0.203	0.875	0.477	0.283	31.39
1	100	−1.213	0.397	−0.858	0.270	1.259	0.570	0.320	33.24
1	150	−1.139	0.367	−0.863	0.264	1.389	0.479	0.381	35.80
1	200	−1.099	0.359	−0.861	0.259	1.463	0.441	0.418	36.91
1	300	−1.059	0.352	−0.858	0.257	1.529	0.423	0.458	37.96
1	400	−1.035	0.353	−0.859	0.258	1.552	0.418	0.476	38.64
2	50	−1.412	0.283	−0.690	0.167	0.865	0.595	0.176	23.61
2	54	−1.399	0.280	−0.702	0.165	0.894	0.563	0.187	24.73
2	58	−1.374	0.264	−0.712	0.163	0.921	0.534	0.199	25.58
5	40	−1.497	0.158	−0.499	0.104	0.600	0.421	0.113	17.07
10	50	−1.474	0.079	−0.459	0.056	0.565	0.219	0.118	16.51
10	80	−1.419	0.061	−0.538	0.044	0.765	0.141	0.170	20.39
10	150	−1.330	0.047	−0.584	0.035	1.035	0.088	0.246	23.45
10	200	−1.297	0.045	−0.594	0.033	1.143	0.076	0.279	24.13

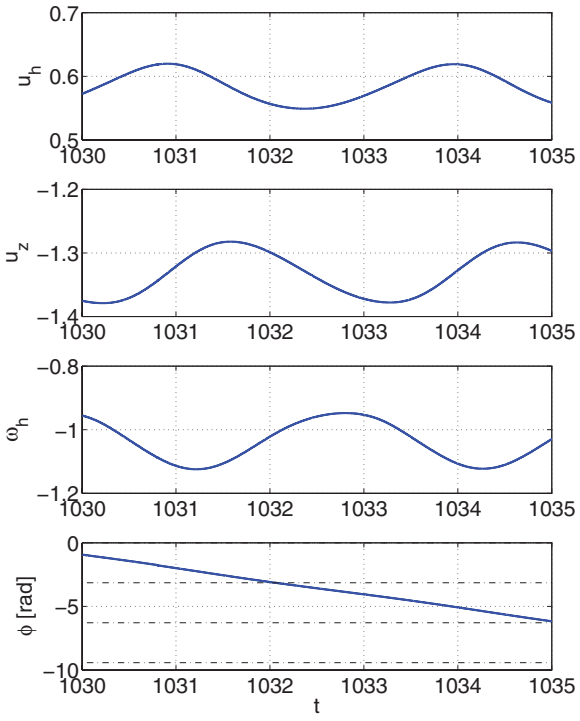

FIG. 11. $m^* = 10$, $G = 150$. For the meaning of symbols, see caption of Figure 9.

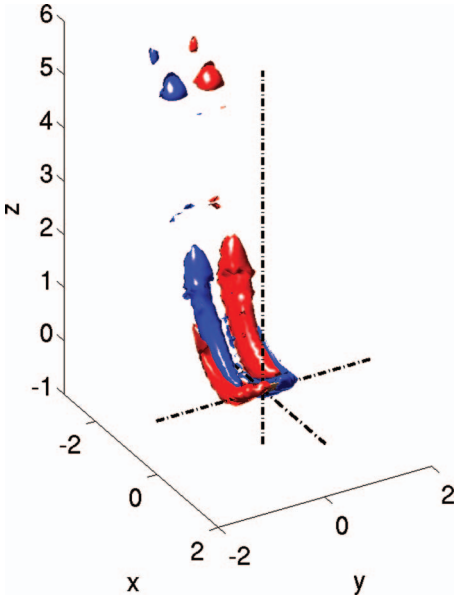

FIG. 12. Tumbling state, $m^* = 0.5$, $G = 160$. Axial vorticity iso-surfaces at levels ± 1.1.

(bottom) for $m^* = 0.25$ at $G = 110$. As can be seen, the disc switches randomly the direction of the rotation and of the side-wise motion (Figure 14).

At the same value of $m^* = 0.25$, but at higher Galileo number $G = 300$, we evidenced a periodic version of the same behavior (see Figure 15). The switching of the sign of the angular and horizontal velocity occurs periodically. The simulation of Figure 16 was restarted using a periodic tumbling state as an initial condition. A long stage of tumbling that could be mistaken for an established state persists for many periods. It is, however, perturbed by a rapidly growing sub-harmonic modulation resulting eventually in a periodic change of the tumbling direction. This results again in a zig-zagging trajectory. In many respects this state resembles the low frequency zig-zagging state evidences for ascending spheres. It can be assumed that, similarly as the zig-zagging regime of the sphere, the stability of this peculiar regime is likely to be very weak. We decided not to introduce a specific classification for this state. Moreover, the planarity of the trajectory was found to be slightly unstable which lets expect the trajectory to become helical at a distant time horizon (see Sec. III A 5).

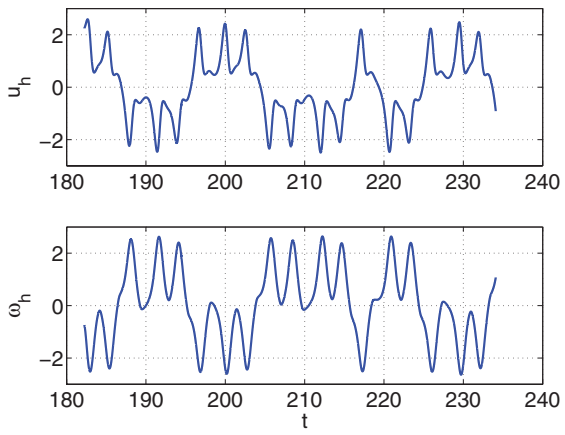

FIG. 13. Intermittent state, $m^* = 0.25$, $G = 110$. (Top) Horizontal component of the velocity; (bottom) the angular velocity ω_h.

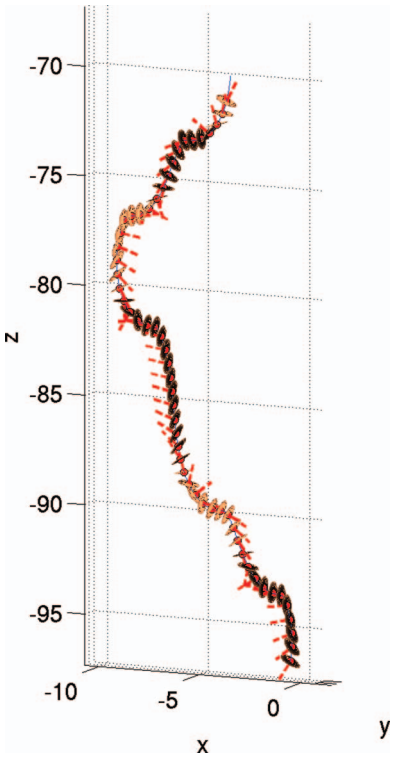

FIG. 14. Intermittent state, $m^* = 0.25$, $G = 110$, z—vertical position, and x, y—horizontal positions as multiples of d. A half-axis of the disc is represented by the dashed line.

4. Quasi-vertical states

We found two distinct states characterized by a very small amplitude of the horizontal velocity component and of other characteristics distinguishing them from a vertical fall (ω_h and ϕ), namely, a periodic and a chaotic state. We call them the quasi-vertical periodic (QVP) and chaotic (QVC) states, respectively. A quasi-vertical periodic state resembles the periodic flutter. It is also planar. However, the Strouhal numbers are equal to about 1/3 the Strouhal numbers of the large amplitude flutter and the amplitude of the horizontal component of the velocity is small and its maximum observed value was $u_{hmax} < 0.05$. As a consequence, the amplitude of the horizontal displacement of the disc was also very weak $\Delta s < 0.07d$. The maximum inclination ϕ_{max} of the disc never exceeded 3° for all observed cases.

Figure 17 shows u_h (top), u_z (middle), and ϕ (bottom) for $m^* = 0.05$ at $G = 80$ as functions of time. The linear growth rate of the amplification is $\gamma = 0.0228$. The amplitudes of the horizontal component of the velocity, as well as of the inclination angle begin to saturate to small asymptotic values $u_h \approx 0.022$ and $\phi_{max} \approx 0.009$ (rad) ($\approx 0.5^\circ$). The Strouhal number is equal to $St = 0.107$.

Very weak oscillations of the disc are hard to distinguish from external disturbances in experiments. For $m^* = 0$, the interval of periodic quasi-vertical regimes is very limited and the trajectories become chaotic and fully three dimensional. Figure 18 shows the onset of a typical chaotic quasi-vertical trajectory. For all the investigated cases, the trajectories displayed only a weak departure from the vertical trajectory (smaller than 0.1d) for a vertical distance of $100d$. The maximum inclination angle was always $\phi_{max} < 5^\circ$ and the horizontal component of velocity was $u_{h_{max}} < 0.08$. Subsequently, for higher Galileo numbers the periodic flutter, described above, appears. We found that for $m^* = 0$ the flutter co-exists with the quasi-vertical chaotic state for $G \approx 130$–180 and for $m^* = 0.05$ it co-exists with the quasi-vertical periodic and the steady vertical state. It can be conjectured that the competition of two pairs of complex conjugate eigenvalues related to the frequency of

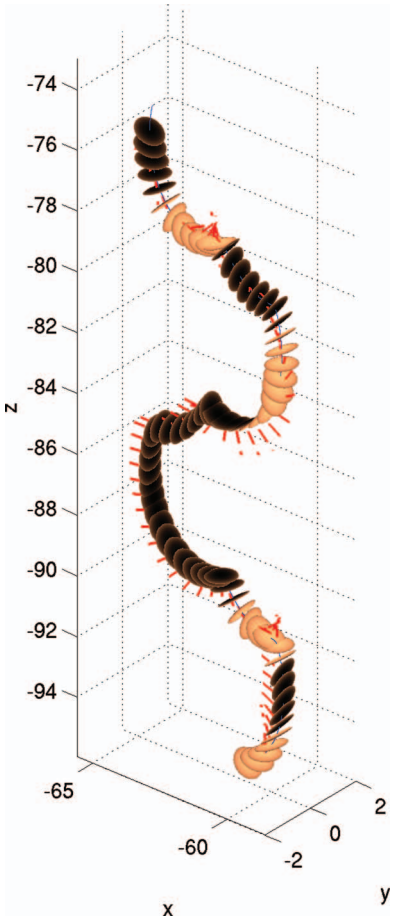

FIG. 15. Tumbling-zigzagging state, $m^* = 0.25$, $G = 300$, z—vertical position, and x, y—horizontal positions as multiples of d. Note the tumbling evidenced by representing a half axis of the disc.

quasi-vertical periodic and of the periodic fluttering state might explain the early onset the quasi-vertical chaotic state.

The Strouhal numbers based on the frequency of oscillations of u_h for the quasi-vertical periodic states and the periodic flutter as a function of the Galileo number for $m^* = 0$ are represented in Figure 19. For infinitely light discs, the chaotic state is, moreover, present. Two dashed-dotted lines delimit the quasi-vertical chaotic region. The blue dashed line marks the lower limit of stability of the periodic flutter.

5. Three-dimensional states

Zhong *et al.*[10] evidenced experimentally the existence of "spiral" states in the transition scenario of thin discs. They identified two new types of motion, which they called spiral and transitional states, for discs having small moments of inertia I^*. They observed that the initial planar zig-zag motion is destabilized by the growth of a secondary oscillation in the normal direction. The disc starts to rotate about its symmetry axis which leads eventually to a spiral motion. They characterized the found states using a factor ϵ expressing the ratio of the short axis to long axis of an ellipse resulting from the projection of trajectories on a horizontal plane described during one period. The planar motion corresponds to $\epsilon = 0$ and the spiral motion corresponds to $\epsilon = 1$. The transitional states correspond to intermediate values of ϵ.

We also evidenced similar states in our DNS. For $m^* = 0.05$ (which corresponds to $I^* = 3.12 \times 10^{-3}$) we observed that the planar zig-zag state quickly becomes unstable and a

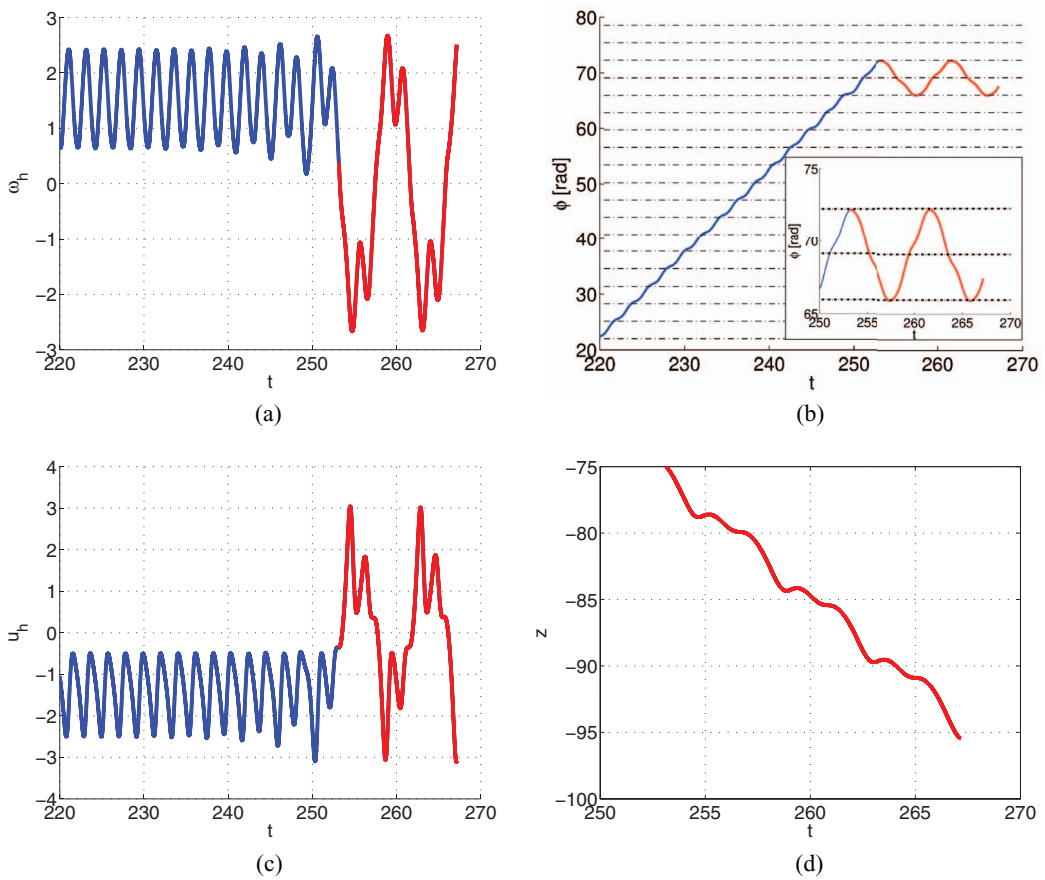

FIG. 16. $m^* = 0.25$, $G = 300$. Sub-harmonic transition from the tumbling to the tumbling-zigzagging state. (a) Angular velocity ω_h; (b) inclination angle ϕ in radians; (c) horizontal component of the velocity u_h; and (d) vertical position z. The dotted lines in the graph (b) mark the rotation by $k\pi$, where $k = 1, 2, ...$

transition to the spiral state takes place. Figure 20(a) shows the spiral trajectory found for $m^* = 0.05$ at $G = 300$. It is characterized by a constant angle of inclination of the disc equal to $\phi \approx 25^\circ$. The disc rotates about its axis with a constant angular velocity $\omega_z = 0.635$. The projection of the trajectory on the horizontal plane is a circle of radius $r/d = 0.37$. The vertical component of

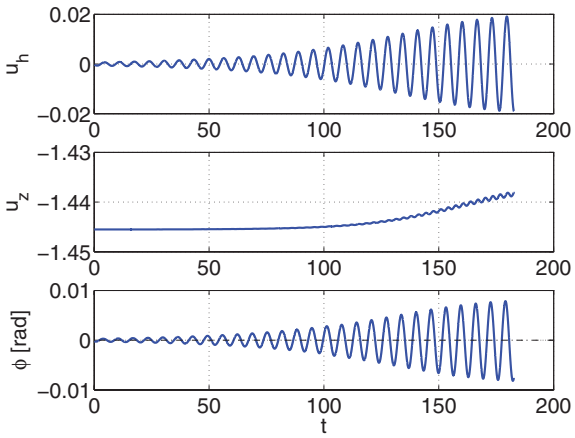

FIG. 17. $m^* = 0.05$, $G = 80$. u_h: horizontal component; u_z: vertical component of the non-dimensionalized velocity; and ϕ: inclination of the disc defined as the angle between the disc axis and the vertical direction in radians.

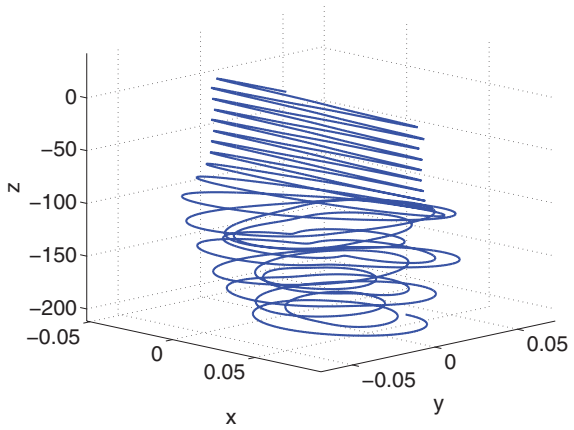

FIG. 18. $m^* = 0.0$, $G = 120$. Quasi-vertical chaotic trajectory of the disc. z—vertical position and x, y—horizontal positions as multiples of d. Note the very small horizontal scale.

velocity is equal to $u_z = -1.07$. The Strouhal number based on the frequency of oscillations of the horizontal component of the velocity and on the vertical velocity is $St = 0.533$. Figure 20(c) shows the wake by representing the axial vorticity iso-surfaces at levels ± 0.35.

For other investigated values of $m^* < 0.5$ the departure of trajectories from the plane was extremely slow especially for low values of Galileo numbers and led to transitional states, which can all be expected to reach the established spiral motion. Zhong *et al.*[10] reported the existence of three-dimensional states only for $m^* < 0.13$. We found that for a sufficiently high Galileo number the planar trajectories become unstable whatever the non-dimensionalized mass $0 \leq m^* \leq 10$. In particular, we found that the tumbling state has its spiral counter-part, which can be called spiral tumbling state (ST). Its trajectory, found for $m^* = 0.5$ at $G = 400$, is represented in Figures 21(a) and 21(b). The projection of the trajectory on the horizontal plane describes a large circle of radius $r/d = 13$. The pitch angle of the spiral is equal to $\alpha = 42.5^\circ$. Other characteristics are summed up, together with those of the spiral state described in Table V.

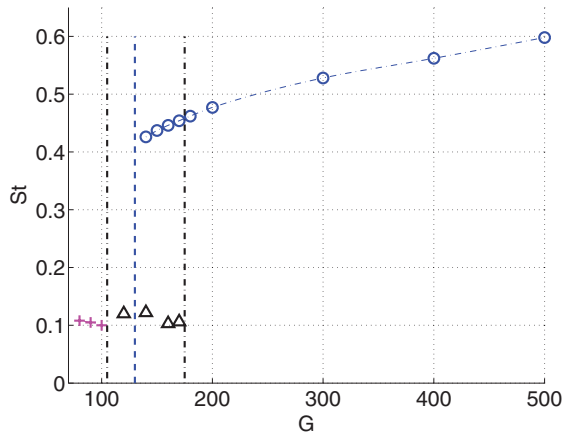

FIG. 19. Strouhal number as a function of the Galileo number. Crosses—quasi-vertical periodic state; triangles—quasi vertical chaotic state, the Strouhal number was estimated using the main peak of the frequency spectrum and the mean vertical velocity; and circles—periodic flutter state. The dashed-dotted lines delimit the interval of quasi-vertical chaotic states, the dashed line represents the lower limit of stability of the flutter.

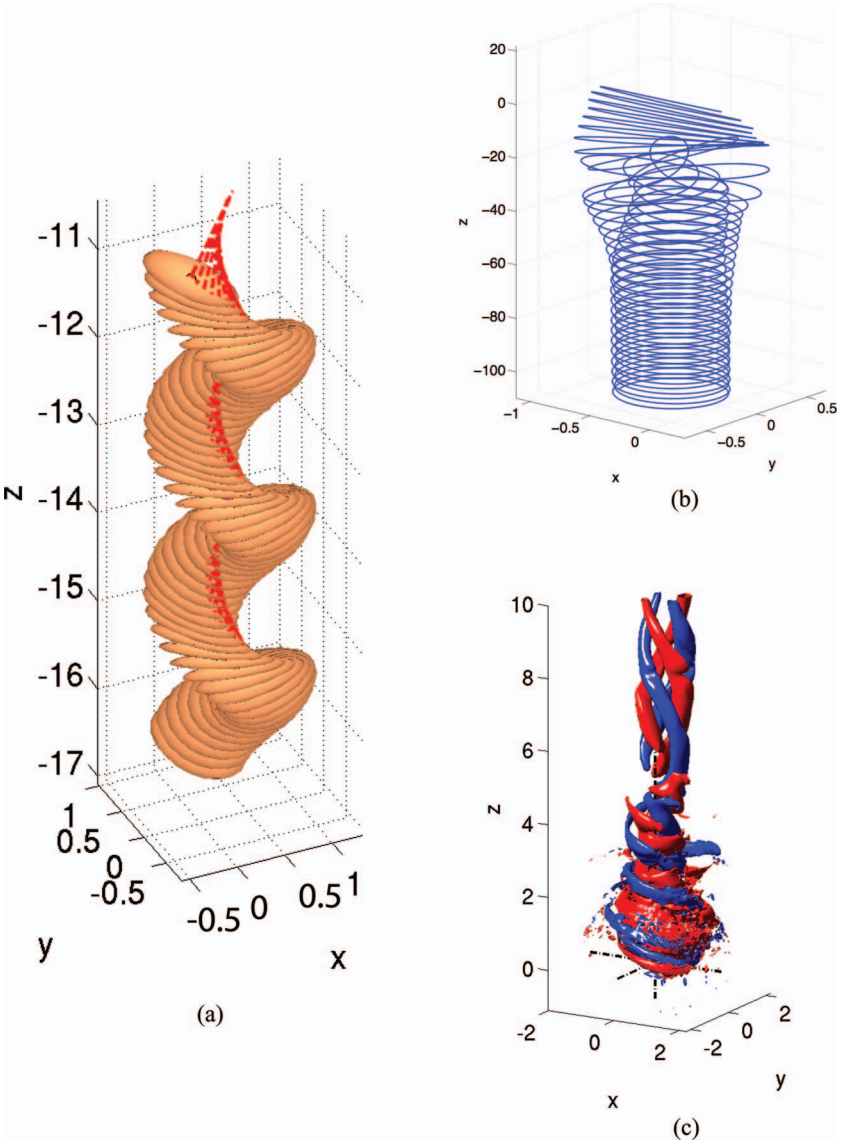

FIG. 20. $m^* = 0.05$, $G = 300$: spiral state. (a) Motion of the disc; the disc axis is represented by the dashed line. (b) Trajectory of the disc center showing the transition from planar periodic fluttering state to a spiral one. (c) Axial vorticity iso-surfaces at levels ± 0.35.

B. State diagram

We swept the whole (m^*, G) parameter space in the range represented in the state diagram of Figure 22. The diagram features only stable states observable experimentally or obtained numerically as converged asymptotic states in fully 3D simulations without any restriction of the solution space. For example, the mathematical solution corresponding to a vertical fall over the edge (the disc axis being horizontal) has never been found to be stable. The simplest state, stable at low values of G, is the vertical fall of horizontal disc at a constant terminal velocity. The disc axis remains parallel to the vertical direction and all flow characteristics are steady. The state is a fixed point in terms of bifurcation theory. For the case of a disc even the primary instability presents complex features, in contrast to a spherical body (for which it was of a regular type). This instability was investigated for increasing G for 10 values of m^* ranging from zero to 10.

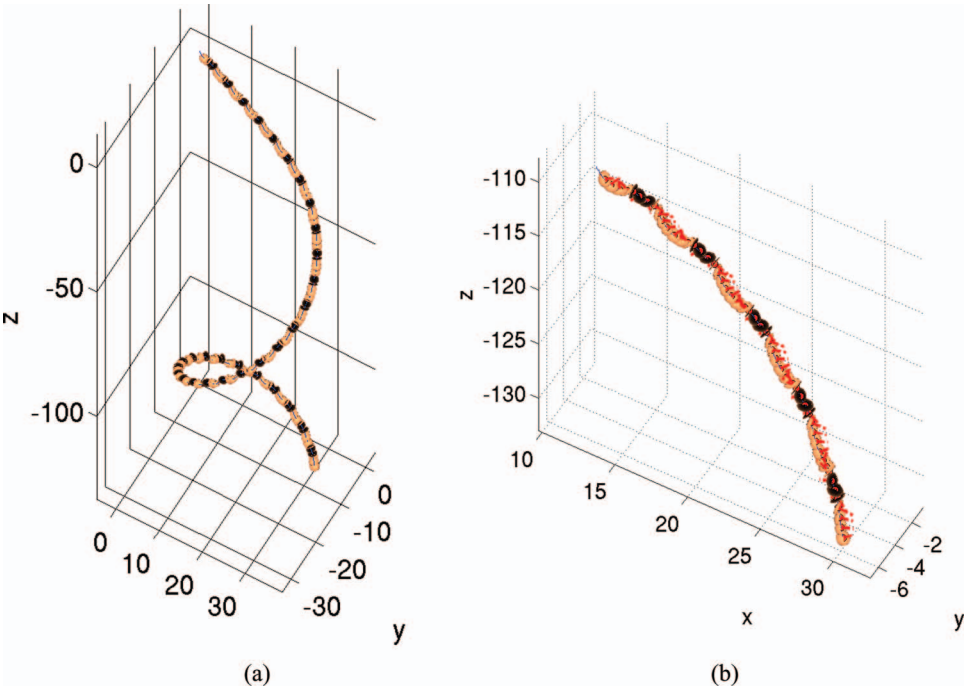

FIG. 21. $m^* = 0.5$, $G = 400$; spiral tumbling state. (a) The disc is enlarged by a factor of 2. (b) Detail of figure (a). The disc is on scale in this figure.

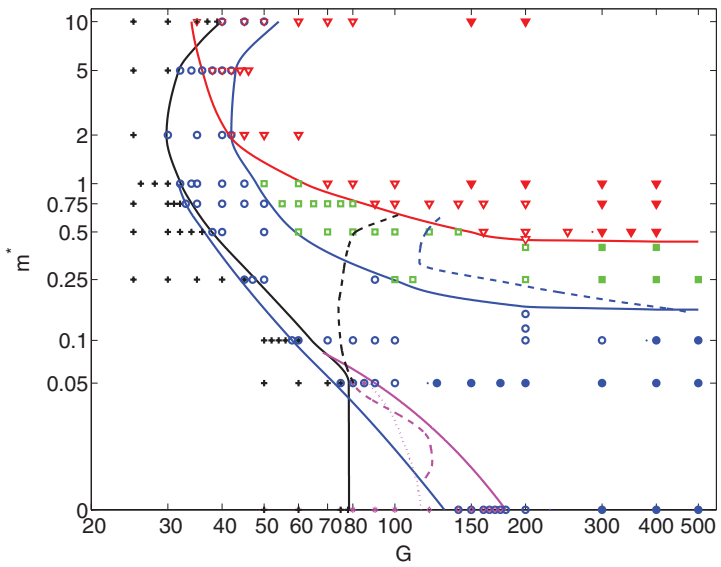

FIG. 22. State diagram in the G–m^* plane. The symbols denote regimes investigated by simulations. The full lines delimit the stability domains. Black: vertical fall (crosses) and limit of stability of the vertical fall. Blue circles and blue lines: fluttering state, red triangles and lines: tumbling state. Green squares: intermittent state. Magenta (triangular domain at $m^* < 0.1$)—quasi-vertical states: asterisks—slow periodic and diamonds—chaotic. Three-dimensional (helical) trajectories are represented by filled symbols. Dashed lines are those of Field *et al.*[3] and of Willmarth *et al.*[5] Their colors establish the correspondence with the full lines resulting from the present numerical simulations. For $m^* < 0.1$ we associate the experimentally observed onset of flutter with a transition from a quasi-vertical regime, which explains the magenta color of the dashed line. Note that it falls well within the bistability domain. The horizontal scale is logarithmic and the vertical one is given by $\log(m^* + 0.01)$ so as to allow $m^* = 0$ to be plotted.

TABLE V. Some quantitative data for selected three-dimensional regimes in diagram of Figure 22. ST: spiral tumbling; spiral: spiral state; *Re*: mean Reynolds number; $\Delta Re/Re$: relative amplitude of fluctuations of vertical velocity; *f*: non-dimensional frequency (in units $\sqrt{|m^* - V^*|g/d}$); ϕ: inclination angle of the axis; α: mean angle with respect to vertical direction; and *r/d*: horizontal deviation from the vertical direction: maximum for flutter, constant horizontal radius of trajectory for spiral regimes.

Regime	m^*	G	Re	$\Delta Re/Re$	f	ϕ (deg)	α (deg)	r/d
Spiral	0.05	300	320	0	0.57	24.9	0	0.37
ST	0.5	400	425	0.99	0.26	...	42.5[a]	13

[a]Pitch angle of a spiral trajectory.

The bifurcation responsible for the loss of stability of the steady state is of the Hopf type for all m^*. It is sub-critical for m^* between 0.05 and 1, which implies co-existence of the vertical fall and of the next, fluttering, periodic state in a finite region of the phase space. The bistability is represented in diagram of Figure 22 by tracing the upper stability limit for the steady vertical state (black line) and the lower stability limit (blue line) of the fluttering state. The latter has also an upper stability limit visualized, again, by a blue line which does not coincide with the lower stability limit of the next—tumbling state. Where a supercritical bifurcation separates two states (and there is no bistability) the separation line has the color of the left state (stable at lower Galileo numbers). For example, for $m^* > 1$ the upper stability limit of the vertical and the lower stability limit of the flutter coincide and are represented in black. The bistability poses the problem of dependence of the final state on the initial conditions or, in other words, on the attraction basin. It was tracked by increasing and then decreasing the Galileo number while using the end of one simulation as the initial condition for the next one. The stability of asymptotic states was monitored using one of the above-mentioned quantities, mostly the horizontal velocity.

As can be seen in the state diagram (Figure 22) the case of $m^* = 10$ is peculiar. The primary bifurcation also leads to the periodic fluttering state. However, the next bifurcation, yielding the tumbling state, is strongly sub-critical. As the result, the tumbling coexists with both the fluttering and the vertical state in a very significant interval of Galileo numbers. The region of co-existence of the periodic flutter and of the tumbling state extends for $2 < m^* \leq 10$. Its lower and upper limits are marked by the red and blue lines in the diagram, respectively.

For $m^* < 0.05$ the primary bifurcation is also super-critical but yields completely different behavior than for $m^* \geq 0.1$. A very weakly oscillating fluttering state sets in and rapidly becomes chaotic. The very small periodic and chaotic oscillations make the movement of the disc practically indistinguishable from vertical motion. For this reason we called these states quasi-vertical periodic and quasi-vertical chaotic (QVP, QVC) in Sec. III A 4. The data in Table VI show that they are virtually unobservable experimentally because the trajectory deviates from a straight vertical at most by a few percent of the disc diameter and the amplitude of the disc oscillations barely exceeds 1°. The domain of quasi-vertical states significantly delays the onset of a visible flutter. For $m^* = 0$, we evidenced that the quasi-vertical chaotic state persists until $G \approx 180$, above which strong oscillations with higher frequency (flutter) set in. This experimentally observable flutter co-exists with quasi-vertical chaotic states. The lower limit of the interval of bistability of these two states is equal to $G \approx 130$, which agrees very well with the threshold found[8] for thin discs $\chi > 20$ for small values of I^*. It can be assumed that the quasi-vertical state is responsible for the delay of

TABLE VI. Some quantitative data for selected quasi-vertical periodic states. For the meaning of the symbols see caption of Table III.

m^*	G	$\overline{u}_z$	Δu_z	Δu_h	$\Delta \omega_h$	Δs	St	ϕ_{max} (rad)
0	90	−1.439	0.003	0.046	0.019	0.043	0.105	0.019
0	100	−1.444	0.004	0.055	0.030	0.061	0.100	0.022
0.05	85	−1.436	0.002	0.036	0.014	0.037	0.107	0.015

the onset of oscillations observed in experiments. It can also be expected that the experimentally observed threshold will be sensitive to experimental noise. For $m^* = 0.05$ the scenario is similar to that observed for $m^* = 0$. The first bifurcation leads to the quasi-vertical periodic state, characterized by a low frequency and a small amplitude. This state is than directly replaced by a regular periodic flutter (higher frequency, significant amplitude). The quasi-vertical chaotic state was not observed at this value of m^*. By decreasing the Galileo number, we found this periodic state to co-exist with the quasi-vertical periodic and with the steady vertical states.

The state diagram (Figure 22) shows that the transition scenario of the falling discs is dominated by three ordered states: steady vertical fall and two periodic states (limit cycles), the fluttering state and the tumbling state. DNS makes it possible to dissipate all doubts about the periodicity of the tumbling state. The three dominant stability domains mentioned present overlaps related to sub-critical bifurcations and, at the same time, leave a significant domain, that of intermittency, uncovered. Such a situation has not been observed for a spherical body. The red line in Figure 22 delimits the region where the tumbling state is stable. The position of the separation lines was deduced by extrapolation of the amplitude of oscillations of the flutter as can be seen in Figure 6. Only ordered states are represented in this manner. As a consequence, the domain of the intermittent state, considered as resulting from the absence of stability both of the flutter and of the tumbling, is delimited by the blue and red lines. At lower Galileo numbers, all trajectories except those of the quasi-vertical chaotic state found for $m^* = 0$, are plane. At higher Galileo numbers, two types of helical trajectories (description is given in Sec. III A) arise. They are closely related to the neighboring plane trajectories: the spiral trajectories[10] result from the destabilization of the flutter and the new helical tumbling results from the planar tumbling state. They are represented by filled symbols of the same shape as that used for the corresponding plane trajectory.

The state diagram of Figure 22 also features the stability limits of the paper by Field *et al.*[3] For the transformation of the Reynolds numbers of their diagram[3] to Galileo numbers, the Reynolds-Galileo number dependence of the numerical simulation has been used. Due to the difficulty of controlling the initial condition in experiments, the sub-critical features remained, so far, unobserved. The upward shift of the onset of flutter for light discs (small m^*) can now be explained by the onset of quasi-vertical, experimentally unobservable, regimes. Note that the dashed magenta line in Figure 22 falls well inside the bistability region of quasi-vertical and fluttering states. At $G > 100$, note the very good agreement of the lines delimiting the intermittent state from the side of both lower and higher non-dimensionalized masses. The fact that no unsteady states have been found experimentally below $G = 80$ is intriguing. We tried to find an explanation by comparing the characteristic vertical scale of amplification rates of the instabilities leading from the vertical fall to unsteady states to the vertical height of the experimental setup[3] but the amplification rates are large enough even at low Galileo numbers for the observation of the unsteady states to be expected even on limited vertical distances. The question has to be clarified in the future by a campaign of simultaneous experiments and simulations. Discs with high inertia ($m^* > 1$) have not been investigated previously but the trend towards tumbling has been reported.

The most salient features of the state diagram can be explained in terms of inertial effects. The bi-stability of the flutter and of the vertical ascension (for very small m^*, of the flutter and of the quasi-vertical regime) can be understood as a consequence of the strong oscillating movement of the fluid keeping, by inertia of the fluid, its stability below the primary instability threshold. This effect is limited to regimes for which the inertia of the fluid dominates that of the solid. Conversely, at high values of non-dimensionalized mass ($m^* \geq 5$), the inertia of solid dominates that of the fluid. As the result, there exists an interval of Galileo numbers at which the flutter still remains stable but at which the fluid cannot stop the rotation once the tumbling regime gets established. The effect of inertia on the scenario is particularly relevant at high Galileo numbers. Indeed, the separation lines marking the thresholds between the stability domains of the flutter, intermittency and tumbling regime become practically independent of the Galileo number. The disc behaves much like a nonlinear pendulum. In Figures 3, 4, 9, and 10 it can be seen by comparing the plots of the torque and of the inclination angle of the disc axis that the hydrodynamic torque plays a similar role as the torque driving a nonlinear pendulum, i.e., in the oscillating regime (flutter), it tends to reduce the inclination and, in the tumbling regime, it slows the rotation once per period at a position at which the disc axis is

horizontal. "Light discs" ($m^* > 1.2$) do not have enough inertia to rotate over the edge and therefore they oscillate. "Massive" discs have enough inertia to remain in the tumbling regime. The nonlinear effects due to the fluid–solid interaction are at the origin of the intermediate regime at which none of both states is stable and the system switches intermittently (or sometimes periodically) from flutter to tumbling.

C. Remarks

DNS provides more complete information on the transition scenario than can be obtained by experimental observations. The agreement between the numerical and experimental data is not perfect but is quite reasonable, especially as far as stability limits of fluttering and tumbling states at higher Galileo numbers are concerned. However, the absence of experimental observations of non-vertical states at small Galileo numbers ($G < 80$) and at larger values of m^* ($m^* > 0.1$) needs to be clarified.

The state diagram does not provide all the relevant information. We have already mentioned the difficulty of observing the weakly oscillating chaotic regime for light discs. An explanation cannot be given without quantitative indication of the amplitudes of the oscillations of such states. Table VI shows that the trajectories of the quasi-vertical states actually deviate from a vertical line by only a few percent of the disc diameter and the amplitude of disc rotation remains of the order of a degree. Laboratory observations of falling discs are limited by the vertical height of the experimental setup, as a consequence, slowly growing instabilities remain unnoticed. Therefore, amplification rates may represent valuable information. The experimental literature (see the review[7]) does not report the existence of bistable states. This can be explained by the fact that in experiments it is difficult to control precisely the initial and boundary conditions. Moreover, the fluid medium is not perfectly quiescent, which perturbs the system and promotes the development of instabilities. Some quantitative characteristics, such as amplitude of oscillation of the disc axis during the flutter, are very likely reproducible in experiments. For this purpose we added the tables appearing in Sec. III A.

IV. CONCLUSIONS

We revisited, completed, and extended the widely known phase diagram of Field *et al.*[3] by data concerning very light and very dense discs. We found the four states reported earlier. Our instability thresholds are to a large extent in good agreement with the experimental data. For $m^* < 0.1$ we found a domain of co-existence of quasi-vertical and fluttering states. Its lower limit also agrees very well with the experimental data. The weakly oscillating states, which are unobservable in experiments, explain the delay of the transition observed for small m^* already by Willmarth*et al.*[5] for discs and recently by Fernandes *et al.*[8] for flat cylinders of aspect ratio $\chi \geq 10$. We also report a similar trend as in experiments to observe tumbling states for higher values of m^*. However, we found significant differences in the onsets of instabilities for intermediate values of m^*. Our DNS indicate that the transition to the periodic fluttering and to the intermittent states occurs earlier than in experiments. This delay of onset of instabilities in experiments requires further explanation. We dissipated all doubts if the tumbling state is periodic. In our simulations, we evidenced also non-planar states reported experimentally very recently by Zhong *et al.*[10] In addition, we found a new spiral tumbling state.

The presented numerical results significantly complete and clarify the transition scenario of falling homogeneous discs for all practically realizable non-dimensional masses and for Galileo numbers covering the most significant stages of the transition. DNS yields details not only on the dynamics of the solid body but also on that of the wake and its structure. The knowledge obtained is also of fundamental importance for the understanding of complex multi-particle flows involving non-spherical particles. The numerical method can provide, due to its accuracy, a useful tool for the benchmarking of numerical codes designed for multi-particle flow simulations.

ACKNOWLEDGMENTS

The work was partly supported by the French Government Grant No. ANR-09-BLAN-132 OBLIC. Jan Dušek would like to thank Vincent Heuveline for raising the subject.

[1] M. Jenny and J. Dušek, "Efficient numerical method for the direct numerical simulation of the flow past a single light moving spherical body in transitional regimes," J. Comput. Phys. **194**(1), 215 (2004).
[2] C. H. J. Veldhuis and A. Biesheuvel, "An experimental study of the regimes of motion of spheres falling or ascending freely in a Newtonian fluid," Int. J. Multiphase Flow **33**(10), 1074 (2007).
[3] S. B. Field, M. Klaus, and M. G. Moore, "Chaotic dynamics of falling disks," Nature (London) **388**, 252 (1997).
[4] G. E. Stringham, D. B. Simons, and H. P. Guy, "The behavior of large particles falling in quiescent liquids," in *Geological Survey Professional Paper* (U.S. Government Printing Office, Washington, 1969).
[5] W. W. Willmarth, N. E. Hawk, and R. L. Harvey, "Steady and unsteady motions and wakes of freely falling disks," Phys. Fluids **7**, 197 (1964).
[6] S. H. Strogatz, *Nonlinear Dynamics and Chaos: With Application to Physics, Biology, Chemistry and Engineering* (Addison-Wesley, New York, 1994).
[7] P. Ern, F. Risso, D. Fabre, and J. Magnaudet, "Wake-induced oscillatory paths of bodies freely rising of falling in fluids," Annu. Rev. Fluid Mech. **44**, 97 (2012).
[8] P. C. Fernandes, F. Risso, P. Ern, and J. Magnaudet, "Oscillatory motion and wake instability of freely rising axisymmetric bodies," J. Fluid Mech. **573**, 479 (2007).
[9] F. Auguste, "Instabilits de sillage gnres derrire un corps solide cylindrique, fixe ou mobile dans un fluide visqueux," Ph.D. dissertation (Universit Paul Sabatier, Toulouse, 2010).
[10] H. Zhong, S. Chen, and C. Lee, "Experimental study of freely falling thin disks: Transition from planar zigzag to spiral," Phys. Fluids **23**(1), 011702 (2011).
[11] M. Jenny, J. Dušek, and G. Bouchet, "Instabilities and transition of a sphere falling or ascending freely in a Newtonian fluid," J. Fluid Mech. **508**, 201 (2004).
[12] B. Ghidersa and J. Dušek, "Breaking of axisymmetry and onset of unsteadiness in the wake of a sphere," J. Fluid Mech. **423**, 33 (2000).
[13] M. Chrust, G. Bouchet, and J. Dušek,"Parametric study of the transition in the wake of oblate spheroids and flat cylinders," J. Fluid Mech. **665**, 199 (2010).
[14] M. Chrust, "Etude numrique de la chute d'objets axisymtriques dans un fluide newtonien," Ph.D. dissertation (Universit de Strasbourg, Strasbourg, 2012).